Principle and Control of Radial AC Hybrid Magnetic Bearing

Zhang Weiyu[1,a], Zhu Huangqiu[1,b], Yang Zebin[1,c]
[1]School of Electrical and Information Engineering, Jiangsu University, Zhenjiang, China
[a]zwy_729@163.com, [b]zhuhuangqiu@ujs.edu.cn, [c]zbyang@ujs.edu.cn

Abstract: In the paper, the configuration and principle of the radial AC hybrid magnetic bearings are expounded, and the mathematical models of suspension forces are deduced by using the method of equivalent magnetic circuits. Nonlinearities of suspension forces and cross coupling between the two degrees of freedom are studied further by calculating the suspension forces at different displacements and control currents to validate the feasibility of the mathematical models. Then based on the mathematics models , the digital control system is designed. The hardware based on TMS320F2812 is developed, and the software of control system is developed. The experiments are completed and the test results have shown that the AC hybrid magnetic bearing has good dynamic and static performance.

Keywords: AC magnetic bearing, Mathematical model, Cross-Coupling analysis, Digital control

Introduction

Magnetic Bearings are typical electronic and mechanical products, which can suspend the rotor in the space between the rotor and stator without mechanical contact by the generated magnetic force. According to the type of current driven, magnetic bearing can be classified as AC magnetic bearing and DC magnetic bearing. For the DC magnetic bearing, high cost of power amplifiers are essential for a radial magnetic bearing, for the AC magnetic bearing, only an AC 3-phase power inverter is enough, and has the merits of mature application technology, low cost and small size. According to principle of producing suspension forces, magnetic bearings can be classified as passive magnetic bearing, active magnetic bearing and hybrid magnetic bearing. Hybrid magnetic bearing depends on a permanent magnet to provide the biased fluxes and several electromagnetic coils to supply the control fluxes, so the volume of its power amplifier is much smaller than active magnetic bearing, and this kind of bearing has a compact structure and lower power consumption, meanwhile, larger air gap can be realized due to the permanent magnet biased.

In the paper, a radial AC hybrid magnetic bearing is presented. The radial AC hybrid magnetic bearing incorporates the merits of AC stimulating and permanent magnet fluxes biasing. Based on introduction of configuration and principle, and the mathematical models of suspension forces are deduced. Nonlinearities of suspension forces and cross coupling between the two degrees of freedom are studied. The hardware of digital control system based on TMS320F2812 is designed, and the software of control system is developed using C language and assemble language in the C2000 development environment. The experiments have shown that the AC hybrid magnetic bearing has good dynamic and static performance.

Configuration and Principle

Configuration of Radial AC Hybrid Magnetic Bearing. Fig. 1 shows the configuration of radial AC HMB, which consists of two radial stators with three poles, three radial control coils, a rotor, a shaft, an aluminum ring and a permanent magnet ring magnetized axially. The permanent magnet provides the bias fluxes and 3-phase coils provide control fluxes of

the radial HMB. Radial stators are made of stacked Silicon-Steel Sheets, and the permanent magnet material is Nd-Fe-B.

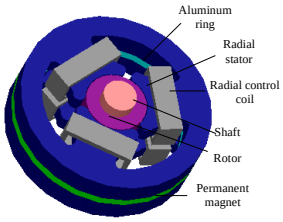

Fig.1 structure of radial AC HMB

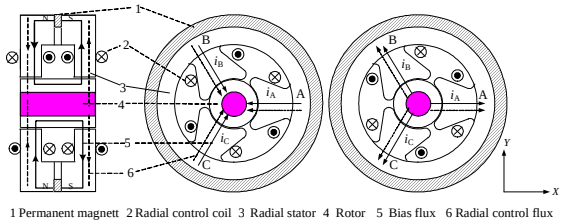

Fig.2 Configuration of radial AC HMB

Principle of Radial AC HMB. The magnetic fluxes path of radial AC HMB is presented in Fig. 2. In Fig. 2, A, B and C represents each pole's position respectively, i_A, i_B and i_C are the radial control currents, respectively. The real lines with arrows represent the static bias fluxes generated by the permanent magnet, which start from N-pole of the permanent magnet, flow through one side of the stator, the radial air gap, the rotor, the other side of the stator, then go back to S-pole of the permanent magnet. The dashed lines with arrows represent the control fluxes generated by the control coils, the radial control fluxes are conducted by the radial stator, radial air gap and the rotor.

Based on principle of bearingless motor, the condition which must be satisfied in generating radial levitation force: $p_2 = p_1 \pm 1$, p_1 is the number of pole pairs of motor winding, p_2 is the number of pole pairs of torque winding. If p_1=0, p_2=1, the bearingless motor is changed into a radial magnetic bearing with only radial suspension force in fact. Based on the motor theory, balanced 3-phase currents flowing in the 3-phase symmetric windings will produce a rotating magnetic field, thus form a unipolar and incorporated magnetic flux. As the rotor departs from the balance position due to disturbances, the radial position sensors measure the radial offset values of the rotor and transfer the displacement signals to the controller. Then the controller transforms them into control current signals, the power amplifier is driven by the control signals and outputs exciting currents. In this way, the stimulating currents generate control fluxes, which are superposed with the biased fluxes, and the resulting force can be pointed in any direction and suspend the rotor in the ideal balance position.

Mathematical Models

Calculation of the Equivalent Magnetic Flux Path. To simplify calculation of the magnetic fluxes path, only the leakage of the inner and outer annulus of the permanent magnet are considered, the whole fluxes path system is taken as a parallel connection system composed by leakage reluctance and available fluxes. And as well, only the air gap reluctance is considered, the reluctance of the irons and the rotor and the eddy current losses are neglected. Therefore, the equivalent permanent magnet circuit is laid out in Fig. 3.

In Fig. 3, F_m is the magnetomotive force that the permanent magnet provides for outer circuits, ϕ_m is the total magnetic flux that the permanent magnet generates, ϕ_l is the total magnetic fluxes leakage of the permanent magnet, the leakage permeance is G_l, G_{A1}, G_{B1}, G_{C1} and G_{A2}, G_{B2}, G_{C2} describe the one side and the other side of radial air gap permeance, respectively. Supposing that the rotor has positive displacements x and y in the two directions x and y respectively, then the magnetic permeance of each air gap can be calculated as follows.

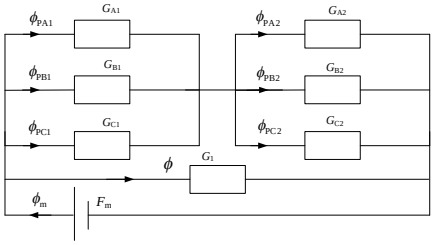

Fig.3 Equivalent fluxes path of the permanent magnet

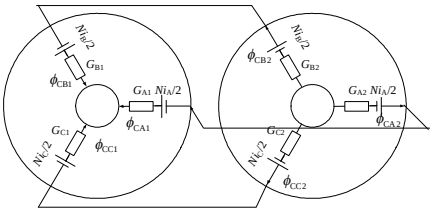

Fig.4 Equivalent flux path of the electromagnet

$$\begin{cases} G_{A1}=G_{A2}=\dfrac{\mu_0 S}{\delta-x} \\ G_{B1}=G_{B2}=\dfrac{\mu_0 S}{\delta+x/2-\sqrt{3}y/2} \\ G_{C1}=G_{C2}=\dfrac{\mu_0 S}{\delta+x/2+\sqrt{3}y/2} \end{cases} \tag{1}$$

where μ_0 is the permeability of the vacuum, S is the radial magnetic pole area, δ is the radial air gap length. Based on the Kirchhoff's laws of the magnetic circuit, the biased fluxes of each air gap in Fig. 1 can be calculated as follows

$$\begin{cases} \Phi_{PA1}=\Phi_{PA2}=\dfrac{\mu_0 S}{\delta-x}\cdot\dfrac{F_m}{2} \\ \Phi_{PB1}=\Phi_{PB2}=\dfrac{\mu_0 S}{\delta+x/2-\sqrt{3}y/2}\cdot\dfrac{F_m}{2} \\ \Phi_{PC1}=\Phi_{PC2}=\dfrac{\mu_0 S}{\delta+x/2-\sqrt{3}y/2}\cdot\dfrac{F_m}{2} \end{cases} \tag{2}$$

Calculation of the Equivalent Electromagnetic Flux Path. In Fig. 2, the control coils are stimulated with certain current, the equivalent fluxes path of electromagnets generated by the coils is shown in Fig. 4, the corresponding equations are shown as

$$\begin{cases} \Phi_{CA1}=\Phi_{CA2}=\dfrac{\mu_0 S}{\delta-x}\cdot\dfrac{1}{2}Ni_A \\ \Phi_{CB1}=\Phi_{CB2}=\dfrac{\mu_0 S}{\delta+x/2-\sqrt{3}y/2}\cdot\dfrac{1}{2}Ni_B \\ \Phi_{CC1}=\Phi_{CC2}=\dfrac{\mu_0 S}{\delta+x/2-\sqrt{3}y/2}\cdot\dfrac{1}{2}Ni_C \end{cases} \tag{3}$$

where N_r is the turns of each radial control coil, i_j is the radial control current(j = A, B, C)

Expressions of Radial Magnetic Attractive Forces. Assuming that the rotor has positive displacements x and y in the x- and y-direction, respectively, then the magnetomotive forces generated by the resulting magnetic flux of each radial air gap can be expressed as the follow

$$F_i=\frac{\left(\Phi_{Pi1}^2+\Phi_{Ci1}^2\right)}{2\mu_0 S}+\frac{\left(\Phi_{Pi2}^2+\Phi_{Ci2}^2\right)}{2\mu_0 S}=\frac{\left(\Phi_{Pi1}^2+\Phi_{Ci1}^2\right)}{\mu_0 S} \tag{4}$$

where i=A, B, C

Substituting Eq. 1, Eq. 2, Eq. 3 into Eq. 4, on the assumption that the rotor has a very small displacement from the radial balance position, Eq. 4 can be linearized as the follow

$$\begin{cases} F_{\mathrm{A}} = F_{\mathrm{A}}\Big|_{\substack{i_{\mathrm{A}}=0\\x=y=0}} + \dfrac{\partial F_{\mathrm{A}}}{\partial i_{\mathrm{A}}}\Big|_{\substack{i_{\mathrm{A}}=0\\x=y=0}} \cdot i_{\mathrm{A}} + \dfrac{\partial F_{\mathrm{A}}}{\partial x_{\mathrm{A}}}\Big|_{\substack{i_{\mathrm{A}}=0\\x=y=0}} \cdot x_{\mathrm{A}} + \dfrac{\partial F_{\mathrm{A}}}{\partial y_{\mathrm{A}}}\Big|_{\substack{i_{\mathrm{A}}=0\\x=y=0}} \cdot y_{\mathrm{A}} = F_{\mathrm{pm}} + K_{ir} \cdot i_{\mathrm{A}} + K_{xy} \cdot x_{\mathrm{A}} \\ F_{\mathrm{B}} = F_{\mathrm{B}}\Big|_{\substack{i_{\mathrm{B}}=0\\x=y=0}} + \dfrac{\partial F_{\mathrm{B}}}{\partial i_{\mathrm{B}}}\Big|_{\substack{i_{\mathrm{B}}=0\\x=y=0}} \cdot i_{\mathrm{B}} + \dfrac{\partial F_{\mathrm{B}}}{\partial x_{\mathrm{B}}}\Big|_{\substack{i_{\mathrm{B}}=0\\x=y=0}} \cdot x_{\mathrm{B}} + \dfrac{\partial F_{\mathrm{B}}}{\partial y_{\mathrm{B}}}\Big|_{\substack{i_{\mathrm{B}}=0\\x=y=0}} \cdot y_{\mathrm{B}} = F_{\mathrm{pm}} + K_{ir} \cdot i_{\mathrm{B}} - \dfrac{1}{2} K_{xy} \cdot x_{\mathrm{B}} + \dfrac{\sqrt{3}}{2} K_{xy} \cdot y_{\mathrm{B}} \\ F_{\mathrm{C}} = F_{\mathrm{C}}\Big|_{\substack{i_{\mathrm{C}}=0\\x=y=0}} + \dfrac{\partial F_{\mathrm{C}}}{\partial i_{\mathrm{C}}}\Big|_{\substack{i_{\mathrm{C}}=0\\x=y=0}} \cdot i_{\mathrm{C}} + \dfrac{\partial F_{\mathrm{C}}}{\partial x_{\mathrm{C}}}\Big|_{\substack{i_{\mathrm{C}}=0\\x=y=0}} \cdot x_{\mathrm{C}} + \dfrac{\partial F_{\mathrm{C}}}{\partial y_{\mathrm{C}}}\Big|_{\substack{i_{\mathrm{C}}=0\\x=y=0}} \cdot y_{\mathrm{C}} = F_{\mathrm{pm}} + K_{ir} \cdot i_{\mathrm{C}} - \dfrac{1}{2} K_{xy} \cdot x_{\mathrm{C}} - \dfrac{\sqrt{3}}{2} K_{xy} \cdot y_{\mathrm{C}} \end{cases} \tag{5}$$

where $F_{\mathrm{pm}} = \dfrac{\mu_0 F_{\mathrm{m}}^2 S}{4\delta^2}, K_{ir} = \dfrac{\mu_0 N F_{\mathrm{m}} S}{2\delta^2}, K_{xy} = \dfrac{\mu_0 F_{\mathrm{m}}{}^2 S}{2\delta^3}$

F_{pm} is the magnetomotive force generated by the permanent magnet flux in each radial air gap, whose value is the same in each radial air gap when the rotor is in the balance position, k_{ir} is called as radial force-current coefficient, k_{xy} is called as radial force-displacement coefficient. All of the F_{pm}, k_{ir} and k_{xy} are constants in the event of the configuration of the magnetic bearing and the balance position of the rotor is determined.

$$\begin{bmatrix} F_x \\ F_y \end{bmatrix} = \begin{bmatrix} 1 & -\dfrac{1}{2} & -\dfrac{1}{2} \\ 0 & \dfrac{\sqrt{3}}{2} & -\dfrac{\sqrt{3}}{2} \end{bmatrix} \begin{bmatrix} F_{\mathrm{A}} \\ F_{\mathrm{B}} \\ F_{\mathrm{C}} \end{bmatrix} \tag{6}$$

Substituting Eq. 5 into Eq. 6. The resulting forces in *x*- and *y*-direction can be calculated as follows

$$\begin{bmatrix} F_x \\ F_y \end{bmatrix} = K_{ir} \begin{bmatrix} 1 & -\dfrac{1}{2} & -\dfrac{1}{2} \\ 0 & \dfrac{\sqrt{3}}{2} & -\dfrac{\sqrt{3}}{2} \end{bmatrix} \begin{bmatrix} i_{\mathrm{A}} \\ i_{\mathrm{B}} \\ i_{\mathrm{C}} \end{bmatrix} + \frac{3}{2} K_{xy} \begin{bmatrix} 1 & 0 \\ 0 & 1 \end{bmatrix} \begin{bmatrix} x \\ y \end{bmatrix} \tag{7}$$

The condition for a 3-phase system is applicable.

$$i_{\mathrm{A}} + i_{\mathrm{B}} + i_{\mathrm{C}} = 0 \tag{8}$$

With Eq. 9, Eq. 10 and Eq. 11, the equations of the forces F_x and F_y with the three phase currents as parameters can be obtained

$$\begin{bmatrix} F_x \\ F_y \end{bmatrix} = \sqrt{\frac{3}{2}} K_{ir} \begin{bmatrix} 1 & 0 \\ 0 & 1 \end{bmatrix} \begin{bmatrix} i_x \\ i_y \end{bmatrix} + \frac{3}{2} K_{xy} \begin{bmatrix} 1 & 0 \\ 0 & 1 \end{bmatrix} \begin{bmatrix} x \\ y \end{bmatrix} \tag{9}$$

Analysis of Nonlinearity and Cross-coupling

As can be seen from Eq. 4, the relationships about suspension forces, the displacements and control currents are non linear. Fig. 5(a) and Fig. 6(a) based on the physical model, and Fig. 5(b) and Fig. 6(b) based on the mathematical model are both for analysis about nonlinearity and coupling of suspension forces. From the geometry of the figures we see the trend plots are similar, so the primary mathematical model is correct and Eq. 4 is reasonable. The graphs in Fig. 6(a) and Fig. 6(b) are perfectly symmetrical, they are fully comparable to a DC HMB [1]. So it's easier to find a stable controller for *y*-direction. And the strong asymmetry in *x*-direction as Fig. 5(a) and Fig. 5(b) show is caused by three poles geometrical asymmetrical arrangement of the radial magnetic poles about *y*-axis. A robust controller can handle the nonlinearity and asymmetry problems when the rotor is working in a big air gap. But if the rotor is working near the reference balance position, a linear controller is enough to make the bearing works well.

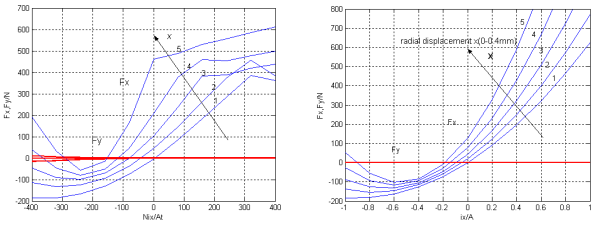

(a) (b)

Fig.5 Calculated current-force graph of the bearing in *x*-direction and *y*-direction when i_y, *y* equal zero
1. *x*=0 2. *x*=0.1 3. *x*=0.2 4. *x*=0.3 5. *x*=0.4

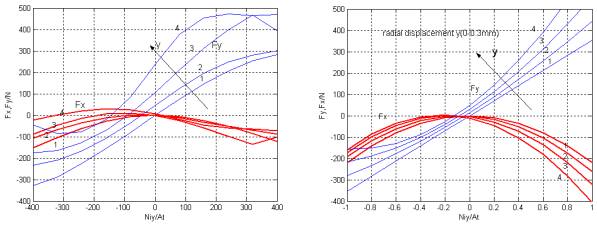

(a) (b)

Fig.6 Calculated current-force graph of the bearing in *y*-direction and *x*-direction when i_x, *x* equal zero
1. *y*=0 2. *y*=0.1 3. *y*=0.2 4. *y*=0.3

Fig. 7(a) and Fig. 7(b) show the relationships about suspension force, the displacement in *x*-direction and *y*-direction in two different lights, the same for Fig. 8(a) and Fig. 8(b). The Fig. 7(a) and Fig. 8(a) can clearly reflect the displacement-force stiffness of the bearing in *x*- and *y*-direction respectively. As can be seen from this couple of waterfall surfaces, the corresponding different displacement- force curves take on nonlinearity with the rise of displacements. Fig. 7(b) and Fig. 8(b) can clearly reflect the suspension forces in *x*- and *y*-direction affected by the displacements in *y*- and *x*-direction respectively due to cross coupling effects. As can be seen from this couple of waterfall surfaces, the surfaces become bended severely with a rise of the displacements in the other direction. But the surfaces near the reference balance position show there is little coupling on the condition of small displacements for the rotor. So based on the linearization mathematical model as showed in Eq. 5, it is feasible to design a linear controller to control the bearing system well.

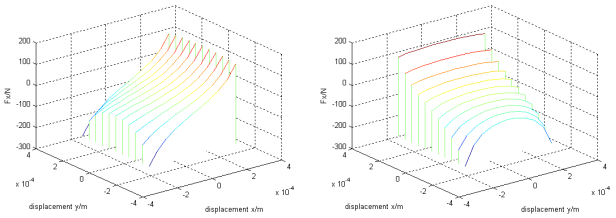

(a) (b)

Fig.7 Relationships among *Fx*, displacement *x* and displacement *y*, $i_x=i_y=0$

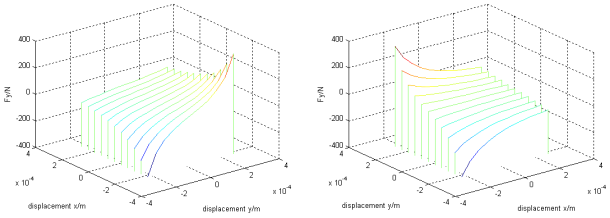

(a) (b)

Fig.8 Relationships among *Fy*, displacement *y* and displacement *x*, $i_x=i_y=0$

Digital Control System

Control Scheme. The picture for this prototype is shown in Fig. 9. The basic control scheme of radial AC HMB is shown in Fig. 10, the whole control system consists of controller, power inverter module, the displacement detection module and prototype ontology. The displacement sensors measure the real radial position of the rotor and output minus feedback signals to Linear Close-loop Controller, compared with the position reference values set previously in the controller, and then the controller will transform the displacements into force signals with PID method. By 2/3 transformation, 3-phase control currents signals i_A*, i_B*, and i_C* are generated, which will produce real control currents (i_A, i_B, and i_C)[5] .The control currents will generate the control fluxes, the suspension force will be generated by the controllable fluxes and makes the rotor suspend in the radial balance position.

Hardware of Digital Control System. To realize the real time control of this digital control system, a high performance digital processor TMS320F2812 is used in this system as

a CPU, which has been used in motor control widely due to its lower cost and losses. Hardware structure of radial AC HMB is shown in Fig. 11.

Software of Digital Control System. The software of this bearing system is constituted by a main program module and several interrupt modules. At the first, the main program finishes the configuration of Watchdog, System clock, A/D conversion and Event management, and then initializes the system variables. Finally, the main program starts the timer, opens the interrupt circulation and waiting the occurrence of interrupts. The interrupt service program module will finish the control arithmetic for the magnetic bearing's magnetic suspension forces. The program flow charts are shown in Fig. 12.

Experimental result. Fig. 13(a) shows the displacement wave forms in *x*- and *y*-direction in the test research on the suspension characteristics of the rotor. The voltage of the balance position for rotor is 1.5V. In the graph, the displacement wave forms in *x*- and *y*-direction

Fig.9 Picture for Radial AC HMB

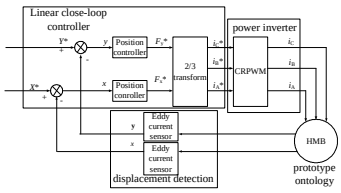

Fig. 10 Control scheme of Radial AC HMB

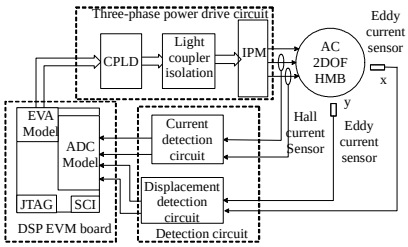

Fig. 11 Hardware structure of Radial AC HMB

exist small fluctuations around the balance position, and show that the system achieved stable suspension. Fig. 13(b) shows the displacement wave forms in *x*-direction in the test research on the floating characteristics of the rotor.

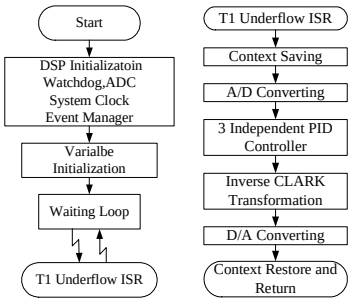

(a) Main program (b) Interrupt program

Fig.12 Program flowchart

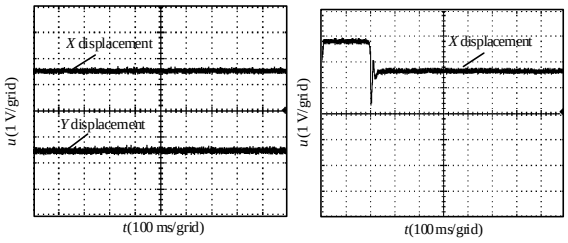

(a) the rotor at suspension stability (d) the rotor at floating state

Fig. 13 Waveforms of experiment results

The rotor floats from the maximum displacement in negative office back to equilibrium position rapidly under the control of current, and show that the system has good performance for the floating.

Conclusion

Based on introduction of configuration and principle of the radial AC HMB, the mathematical models of suspension forces are deduced by using the method of equivalent magnetic circuits. Nonlinearities of suspension forces and cross coupling between the two degrees of freedom are studied. The hardware of and the software of the digital control system are designed, and the experiments are completed and the test results have shown that the AC hybrid magnetic bearing has good dynamic and static performance.

Acknowledgements

This work is sponsored by the National High Technology Research and Development of China (2007AA04Z213), the National Natural Science Foundation of China (60974053), and the Research Fund for the Doctoral Program of Higher Education of China (20093227110002).

References

[1] H.Q. Zhu, S.Q. Yuan, B. Li, Y.K. Sun, D.M. Wang and Y.G. Yan: The working principle and parameter design for permanent magnet biased radial-axial direction magnetic bearing, Proceedings of the CSEE, Vol. 22 (2002), p. 54-58 (in Chinese).

[2] P.T. McMullen, C.S. Huynh and R.J. Hayes: Combination radial-axial magnetic bearing, in Proc. 7th Int. Symp. on Magnetic Bearings, Zurich, 2000, p. 473-478.

[3] C. Redemann, P. Meuter, A. Ramella and T. Gempp: 30kW bearingless canned motor pump on the test bed, in Proc. 7th Int. Symp. on Magnetic Bearings, Zurich, 2000, p. 189-194.

[4] A. O. Salazar, A. Chiba and T. Fukao: A review of developments in bearingless motors, in Proc. 7th Int. Symp. on Magnetic Bearings, Zurich, 2000, p. 335-400.

[5] R. Schoeb, C. Redemann and T. Gempp: Radial active magnetic bearing for operation with a 3-phase power converter, in Proc. 4th Int. Symp. on Magnetic Suspension Technology, Gifu,1997.

[6] L. Mei, Z.Q. Deng, X.S. Zhao, X.G. Wang and X.L. Wang: Parameter design of hybrid axial-radial magnetic bearing based on magnetic flux calculation, Proceedings of the CSEE. Vol. 29 (2009), p.115-121 (in Chinese).

[7] L. Huang, G.Z. Zhao, H. Nian and Y.K. He: Modeling and Design of permanent magnet biased radial-axial magnetic bearing by extended circuit theory, Proceeding of International Conference on Electrical Machines and Systems, Seoul, Korea, 2007.

[8] H.Q. Zhu, Y. Zhou, T.B. Li and X.X. Liu: Decoupling control of 5 degrees of freedom bearingless induction motors using a-th order inverse system method, ACTA Automatica Sinica, Vol. 33 (2007), p.273-278.